Black silicon: Formation in the trampoline mode of ion flow, surface properties, and performance perspectives

9 authors, including:

A. M. Gabovich
Institute of Physics, National Academy of Sciences of Ukraine
444 PUBLICATIONS **2,413** CITATIONS

Vitaliy Kostylyov
V. E. Lashkaryov Institute of Semiconductor Physics National Academy of Science…
123 PUBLICATIONS **502** CITATIONS

Valerii F. Semeniuk
Институт физики НАН Украины
6 PUBLICATIONS **16** CITATIONS

Nadiia I. Semeniuk
Gresem Innovation
5 PUBLICATIONS **15** CITATIONS

Black silicon: Formation in the trampoline mode of ion flow, surface properties, and performance perspectives

Alexander M. Gabovich[1], Vitaliy P. Kostylyov[2], Mykhailo P. Kruglenko[1,3],
Valerii F. Semeniuk[1,3], Nadiia I. Semeniuk[1], Sergei I. Sidorenko[4], Victor I. Styopkin[1],
Alexander I. Voitenko[1], and Svitlana M. Voloshko[4]

[1]*Institute of Physics, National Academy of Sciences of Ukraine, Kyiv 03028, Ukraine*

Email: alexander.gabovich@gmail.com

[2]*V. Lashkaryov Institute of Semiconductor Physics, National Academy of Sciences of Ukraine, Kyiv 03028, Ukraine*

[3]*Gresem Innovation LLC, Kyiv 02660, Ukraine*

[4]*National Technical University of Ukraine "Igor Sikorsky Kyiv Polytechnic Institute", Kyiv 03056, Ukraine*

By irradiating the (111) surface of single-crystalline silicon wafers with Ar^+ ions in the trampoline mode (high-density flows of low-energy ions) and with the assistance of metal initiator atoms, a transition of those wafers into the "black silicon" optical state was stimulated. This state is characterized by low values of light reflectance (less than 2%) from the irradiated wafer side in a spectral interval from 400 to 1000 nm. Scanning electron microscopy studies showed that this is a result of the emergence of a hierarchical submicron/nanoscale structure at the treated surface of the wafers. This transition can be performed only with the assistance of metal initiator atoms simultaneously evaporated from an auxiliary target in the operating chamber. At the same time, the application of metals initiators affects the effective lifetime of the minority charge carriers in the black state silicon, which is crucial for the efficiency of black silicon application in solar cells. Among the examined metals initiators (Al, Cr, Fe, Ni, Mo, and Cu), only the application of copper made it possible to preserve or even increase the value of this parameter. The electrostatic interaction between free electric charges and dipoles (playing the role of excitons in this case) near the interface in a two-layer system was considered theoretically. It was shown how the system parameters affect the preferable location of excitons and their orientation, which can be applied, e.g., to govern the solar cell efficiency. The formation of black silicon in the trampoline mode is environmentally friendly at all production stages.

Keywords: ion-plasma flow, semiconductors, photovoltaics, black silicon, excitons, dipoles, image forces.

1. Introduction

Semiconductor materials provide the basis of modern electronics [1, 2] at least since the transistor invention [3–6]. Moreover, silicon appeared to be the most important material in a new industry, thus starting the "silicon age" of human history [7–11]. It is especially true for artificial photovoltaics [12–16], which became the major competitor with natural photosynthesis [17, 18]. To be effective in light trapping, silicon surfaces should be "black" enough [15, 19–26]. Various methods are used to achieve this goal [21, 23, 27–30]. Nevertheless, even in the optimized set-up, the theoretical (originally, Shockley–Queisser) efficiency limit of 30–35% exists for any single-junction semiconductor device absorbing the incident solar light [26, 31–33]. Hence, fierce competition takes place even for small efficiency gains.

In this connection, a long enough effective lifetime of light-induced excitons is another quantity of extreme importance in solar cells, especially organic ones [24, 33–37]. Both organic and inorganic cells are heterogeneous by definition [33, 35]. This means that the dielectric-constant mismatch between the cell's layers plays a large role in the electrostatic phenomena taking place in such heterostructures. In particular, this is important for the issue of exciton quenching by free charge carriers in the same or adjacent layers [38–42]. Nevertheless, the problem of charge-exciton (charge-dipole) interaction in layered structures

requires the development of a rather sophisticated theory and has been considered properly only recently [43].

Thus this article deals with the key issues of semiconductor physics, where our colleague Vadym Loktev made valuable contributions [44–46]. The outline of the paper is as follows. Section 2 describes our original experiments on the formation of rough silicon surfaces suitable for photovoltaic applications. In particular, the methods of surface processing by ion-plasma flows and the results of sample modification are presented in some detail. In Sec. 3, the theory of charge-dipole interaction in two-layer structures is discussed, and the results of relevant calculations are shown. Section 4 contains a short discussion and conclusions. In the Appendix, we briefly reconstruct the historical appearance of the hole concept in semiconductor physics.

2. Experimental part

2.1. Experimental installation and ion flow generation

The formation of black silicon structures was carried out making use of an ion-plasma flow and on the basis of the original method, which we called the trampoline mode [47]. Its essence is that high-density flows of low-energy ions are used to irradiate the target surface. However, the bombardment of the wafer surface with low-energy ions alone cannot provide a sufficient erosion of this surface to the black silicon state. To achieve the required result, the surface has to retain atoms of some metals (metals initiators) that can start and promote an intensive surface roughening with the formation of hierarchical submicron/nanoscale structures. Such a function of metallic components is similar to their initiating (catalyzing) role in monomer polymerization [48, 49] as well as large-scale GaN rod and nanowire preparation [50].

The schematic diagram of the corresponding installation where those conditions are implemented is shown in Fig. 1. The process chamber was made of non-magnetic chromium-nickel stainless steel. The dimensions of the chamber were chosen as follows: the chamber length of 450 mm and the chamber diameter of 200 mm. Those sizes made it possible to implement effective acceleration of the ion-plasma flow due to the transformation of the electromagnetic helicon waves [51] into the Trivelpiece–Gould surface quasi-electrostatic ones [52–55]. As a result, an ion-plasma flow was created, which was directed from the excitation region of the helicon discharge towards the silicon wafer (8) located on the stainless steel holder (7). The kinetic energies of 20–30 eV of emitted Ar^+ ions entering wafer (8) could be regulated additionally by applying a negative potential difference between holder (7) and the grounded wall of chamber casing (1) (see more details in Ref. 47). The helicon discharge itself was excited using radio-frequency (RF) generator (2) with a frequency of 13.56 MHz and an adjustable power of up to 1200 W. This power was supplied through matching device (3) to two-turn
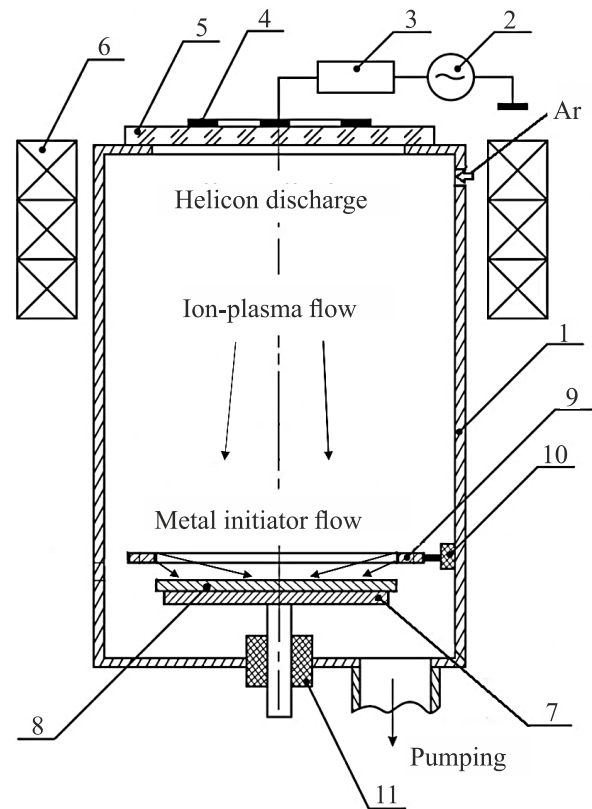

Fig. 1. Schematic diagram of the process chamber: chamber casing (1), RF generator (2), matching device (3), planar antenna (4), quartz window (5), magnetic system (6), wafer holder (7), silicon wafer (8), auxiliary ring metal initiator target (9), insulator of the power supply to the ring target (10), insulator of the power supply to the wafer holder (11).

planar antenna (4). This antenna was mounted on a quartz window (5), through which the RF power was fed into the chamber and which ensured the chamber's interior sealing from the external atmosphere. To excite the helicon discharge and create conditions for the formation of a directed ion-plasma flow, magnetic system 6 was used. Holder (7), on which silicon wafer (8) was fixed, had an outer diameter 2 mm smaller than the wafer diameter.

The preliminary vacuum in the process chamber did not exceed 10^{-3} Pa and was provided by a pumping system, which included an oil-free spiral backing pump and a high-vacuum turbomolecular pump. Plasma-forming Ar gas was injected continuously into the helicon discharge excitation zone of the process chamber through an inlet system with a gas flow regulator; the plasma-forming gas pressure was about 1 Pa.

A dense flow of emitted low-energy Ar^+ ions was directed onto a silicon wafer (8) in order to form a black silicon structure on it, similarly to what was done in our previous studies [30]. Briefly speaking, this structure emerges because the accelerated Ar^+ ions randomly knock out Si atoms and clusters from the wafer's near-surface layers. Those layers are in a non-equilibrium quasi-liquid state under the irradiation with a dense flow of low-energy ions of the plasma-forming

Ar gas (the trampoline mode [47]). Silicon particles sputtered from the mentioned quasi-liquid phase become effectively ionized near the wafer surface due to the "catalytic" activity of metal initiator atoms. The catalytic activity of the latter lies in the fact that they comprise an additional source of electrons to the plasma flow due to the induced ion-electron emission (Auger neutralization). Auxiliary ring target (9) made of the metal initiator is sputtered by bombardment with the same flow of Ar^+ ions.

The silicon particles (atoms and clusters) ejected from the wafer surface are partially re-deposited onto the surface in the form of ions that are concentrated in spots of stronger electric fields, i.e., onto primary hillocks created by the preliminary surface texturing [30]. Thus, a modified rough surface is formed, which strongly reduces the light reflectivity in the visible wavelength range (the black state). It should be noted that the growth of black silicon structures using the trampoline mode is different from known etching methods in which the black silicon structures are formed by removing the material from the surface [56–59] without its following deposition.

2.2. Induced surface structures and sample properties

Black silicon structures were formed by Ar ion flow on the (111) face of *p*-type KDB-9 silicon wafers about 300 μm in thickness and with resistivity $\rho \approx 9$ Ω·cm. The microstructure of the silicon surfaces was examined using an analytical scanning electron microscope Tescan Vega 3 of the fourth generation with a thermo-emissive tungsten cathode. The general preliminary survey was performed at a voltage of 20 kV using detectors of backscattered and secondary electrons. The working pressure in the chamber was not higher than 10^{-3} Pa. The shooting was carried out at an incidence angle of the electron beam of 45° relative to the normal to surface of the studied samples.

The character of obtained surface structures was studied using the scanning electron microscopy (SEM) method [60]. An example of the surface profile micrographs is shown in Fig. 2(a) obtained in the case when stainless steel was applied to dope the wafer. As one can see from Fig. 2(a), hierarchical structures with submicron main features and nanoscale relief are formed on the surface of the silicon wafers. The structural hierarchy of this type was obtained earlier in our studies of both metal [47] and semiconductor [47, 61]. The corresponding spectral dependence of the optical reflectivity coefficient from the irradiated wafer surface is displayed in Fig. 2(b). One sees that the created structure has a reflectance of less than 2% in the light wavelength interval from 400 to 1000 nm.

Our experiments verified that the use of iron, chromium, nickel, and molybdenum as metals initiators makes it possible to create effective light-absorbing surface structures on the silicon wafers. In this case, black silicon is formed whatever the type of the semiconductor conductivity and the crystallographic orientation, in particular, on the
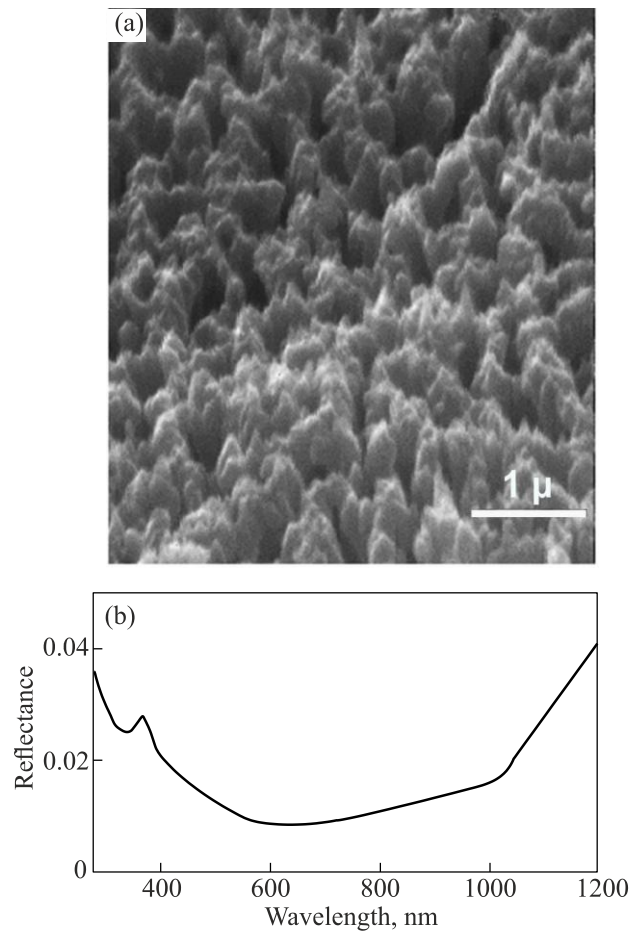

Fig. 2. (a) Scanning electron microscopy (SEM) micrograph of a submicron silicon surface structure with a nanoscale relief. (b) Spectral dependence of the light reflectance from the silicon wafer.

surface of multicrystalline silicon [30]. However, this procedure does not ensure a long enough recombination lifetime τ of nonequilibrium minority charge carriers. Figure 3(a) illustrates how the bombardment with Ar^+ ions affects this parameter in the presence of various metals initiators (namely, Ni for sample 1 and Fe for sample 2). One can see that such processing reduces the τ value, i.e., deteriorates the photovoltaic characteristics of the structure. Similar results were obtained for almost all other examined metals initiators: Al, Cr, and Mo, despite the fact that molybdenum atoms demonstrate the smallest diffusion coefficient in silicon among the given list of elements [62, 63].

Among all researched initiators, the preservation of the parameter τ after the trampoline transformation of the silicon wafer surface into the black state was achieved only when copper was used [Fig. 3(b), sample 1]. Furthermore, the lifetime τ can even be enhanced, e.g., if the heated wafer is irradiated [Fig. 3(b), sample 2]. Probably, high τ values are achieved because copper is one of the highest tolerable metallic impurities leading to the smallest increase of the charge-carrier recombination rate in silicon [64]. The increase of the minority carrier effective lifetime could be caused by a reduction of electron losses in the surface
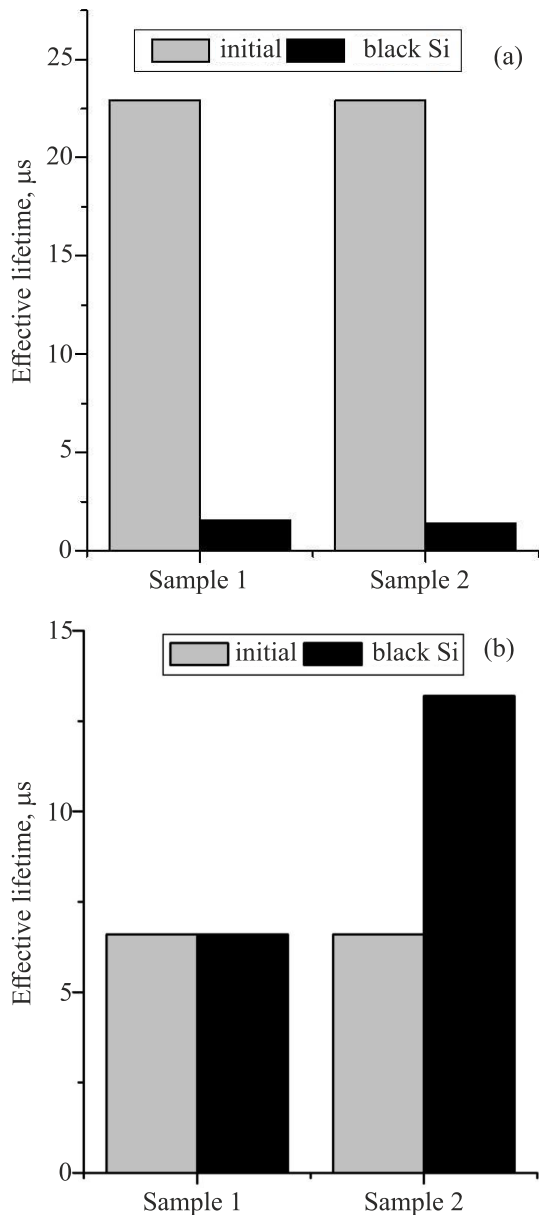
Fig. 3. (a) Change in the effective lifetime τ of excess minority charge carriers before (gray) and after (black) parasitic doping with Ni (sample 1) and Fe (sample 2) metal initiator atoms. (b) The same as in panel (a) but for the Cu-doped silicon wafers Ar^+-irradiated at various temperatures: room temperature (sample 1) and 90 °C (sample 2).

layer that was modified at a higher temperature, most probably, owing to the elimination of interface traps increasing the electron-hole recombination rate [26, 64–75].

The diffusion length and the effective lifetime of the excess minority charge carriers were found by measuring the spectral dependences of the small-signal photo-electromotive force (photo-EMF) [76] near the silicon absorption edge in a light wavelength interval of 400–1200 nm. The method is similar to that described in Ref. 74.

To study the reason for the effective lifetime behavior of the minority charge carriers, the secondary ion mass spectrometry (SIMS) method was applied [77, 78]. A layer-by-

layer SIMS analysis of the composition of the surface of the silicon wafer was carried out on an Ion Tof SIMS IV instrument. Beams of primary O^+ ions with the 2 keV energy and the current 600 nA rastered over an area of 350×350 μm and Ar^+ with the 5 keV energy and the current 10 μA (a current density of 2 μA/mm^{-2}) were applied to irradiate the wafers. Ions $^{28}Si^+$, $^{56}Fe^+$, $^{52}Cr^+$, and $^{58}Ni^+$ sputtered from the wafer by O^+ ions were registered using an MC-7201M spectrometer. The Ar^+ beam provided an average wafer etching rate of about 1.5–2 nm/min. The time dependences of the yields of the sputtered $^{16}O^+$ and $^{12}C^+$ impurities (actually, their distributions across the wafer depth reckoned from the peak tops) were analyzed in this case because their presence in the silicon plates is undesirable since they reduce the lifetime of the minority charge carriers [66, 69, 79, 80].

Primary ions of two kinds were employed for probing because of the limited sensitivity of certain target elements to some incident ions (in particular, Cu atoms to Ar^+ ions and C atoms to O^+ ions). Therefore, the indicated above two-ion bombardment was applied, which allowed us to get maximum information about the chemical composition of the studied samples. The advantages of using primary ions of various types were analyzed in detail in Ref. 81. To be specific, the usage of primary Ar^+ ions made it possible to analyze the wafer-depth distributions of oxygen, ^{16}O, and carbon, ^{12}C, atoms (if any). The same procedure but for the $^{28}Si^+$, $^{56}Fe^+$, $^{52}Cr^+$, and $^{58}Ni^+$ ions can be performed by making use of primary O^+ ions. In addition, the use of primary $^{16}O^+$ ions ensured the increase in the signal intensity from $^{64}Cu^+$ ions by several orders of magnitude as compared to that provided by primary Ar^+ ions [81].

Thus, SIMS measurements of the fractions of various elements across the wafer thickness showed substantial doping of the silicon wafer with impurity atoms (see Fig. 4). Namely, the elements indicated in the legends were probed up to a depth of about 120 nm. The results of SIMS studies using primary Ar^+ ions and stainless steel as the initiator are shown in Fig. 4(a) and those for primary O^+ ions and Cu as the initiator are depicted in Fig. 4(b). Only the data for the most important registered impurities are displayed. The main conclusion from Fig. 4(a) is that the stainless steel components Fe and Cr decrease rapidly with depth, thus not influencing the bulk. Figure 4(b) demonstrates that the distribution of Cu atoms declines with depth even more quickly than the distributions of Fe and Cr do. At the same time, nickels, carbons, and oxygens were registered at the background level.

The SEM micrographs of silicon structures formed under the conditions of Cu-doping from the initiator source are shown in Fig. 5. The black silicon surface structure shown in Fig. 5(a) was formed under the conditions when the silicon wafer was located on the wafer holder at room temperature, and the structure in Fig. 5(b) corresponds to the holder temperature of 90 °C. A comparison of micro-
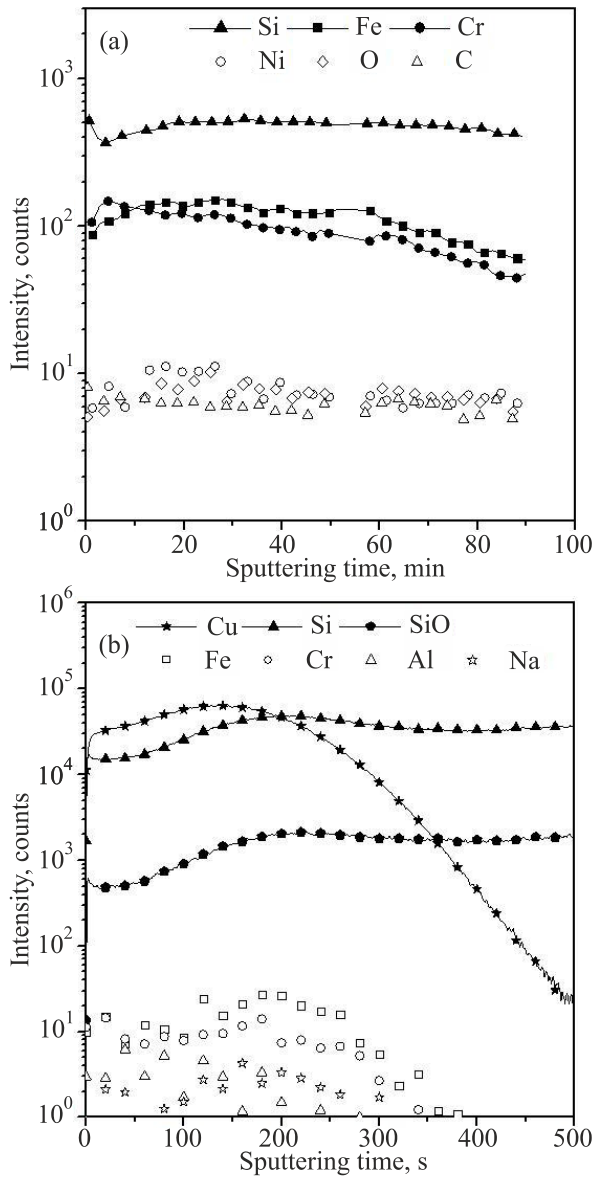
Fig. 4. (a) Secondary ion mass spectrometry (SIMS) analysis, using primary Ar^+ ions, of the composition of a silicon wafer doped with the stainless steel initiator atoms. (b) The same as in panel (a) but for the copper initiator atoms and using primary O^+ ions. See explanations in the text.

Fig. 5. SEM micrographs of black silicon structures formed with the help of copper initiator atoms at the holder room (a) and 90 °C (b) temperatures.

graphs 5(a) and 5(b) with micrograph 2(a) demonstrates that the peaks arising when Cu was used as the metal initiator are more pronounced and regular-spaced than those obtained when stainless steel played this role. Furthermore, the geometric parameters of the peaks (their height and the inter-peak distance) growing at the surface of Cu-doped silicon wafer are very close to those characterizing the peaks appearing at the surface of pure black copper [82, Fig. 5(c)]. This fact testifies to the specific role of copper ions in the formation of black surface structures.

Note that Fig. 5 shows pyramidal submicron formations inclined from the normal, which are formed on the seed structures. This is additional evidence that the creation of
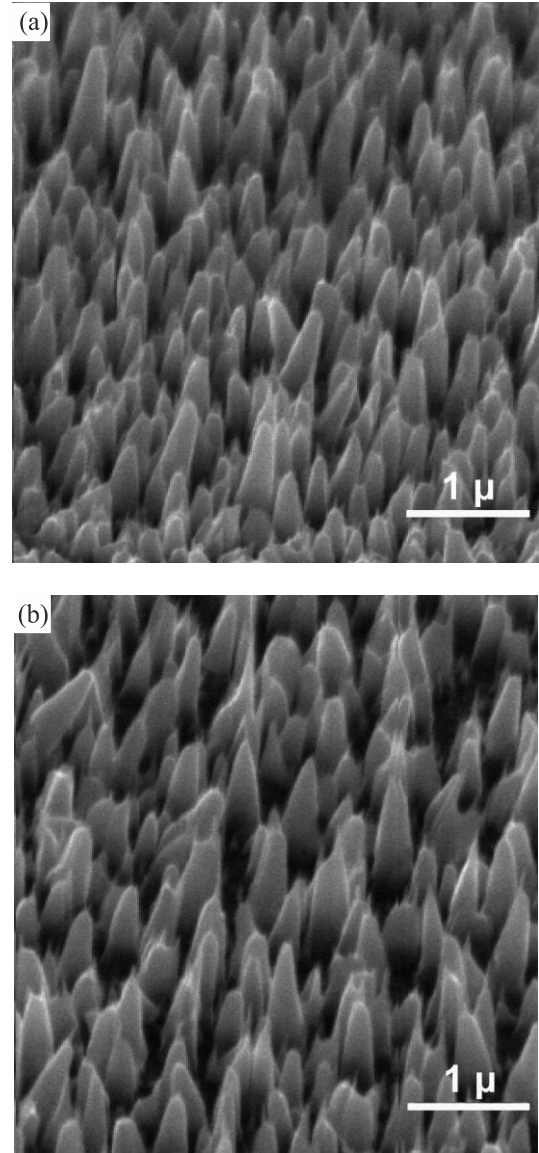
black silicon structures using the trampoline mode occurs as a result of their growth rather than a local silicon removal from the smooth surface of the wafer.

3. Charge-dipole interaction in a two-layer system

As was indicated in the Introduction, exciton properties, including the effective lifetime, can be substantially altered by charged impurities [38–42]. In layered solar cells, such impurities accumulate near the interface (interfaces) due to the action of image forces. The exciton physics is especially important in photovoltaic devices based on organic semiconductors [33, 34, 36]. As a first approximation, the excitons involved can be treated as permanent electric dipoles **P**. The dielectric mismatch between the neighboring layers turns out a very substantial factor in this case [43].

Below, we present an illustration of the free-charge influence on Wannier excitons in two-layer structures.

The direct interaction of the dipole **P** with the point charge Q and the polarization charge created by the charge Q at the interface, on the one hand, and the image-force interaction of the dipole **P** with the polarization charge created by itself at the interface, on the other hand, comprise two independent (in the framework of linear electrostatics!) and competing factors that govern the dipole orientation and bring about a nontrivial result. Namely, the calculations (we used the model of two semi-infinite dispersionless insulators that have different dielectric permittivities and are separated by an infinitely thin plane interface) show that there may appear local minima in the dependence of the dipole energy W on the dipole location **R** and orientation θ, provided that the other problem parameters (the dielectric permittivities ε_1 and ε_2 of the media; the dipole, P, and charge, Q, magnitudes; and the charge location **r**) are fixed. Hence, the dipole may acquire a stable position and an equilibrium orientation somewhere at definite distances from both the charge and the interface.

The results of calculations show that this situation arises when the dipole is in its favorable orientation, i.e., it is attracted by the charge but is repulsed by the interface. It means that the dielectric permittivity of the medium where the dipole is located must be higher than that of the contacting medium. Otherwise, we obtain either a monotonically varying W or an energy barrier with an unstable equilibrium point at its top. Furthermore, the parameters of such minimum configurations are quite different depending on whether the charge and the dipole are located in the same medium or across the interface. For definiteness, let the charge Q be located in medium 1 at the distance $x_Q = 1$ from the interface (here we normalized all distances by the distance X_Q from the charge Q to the interface).

Figure 6(a) illustrates the appearance of the energy well for the dipole with the reduced dipole moment $p = P / (QX_Q) = 1$ located in medium 2 with the dielectric permittivity ε_2 higher than the dielectric permittivity ε_1 of medium 1 where the charge Q is positioned $(\varepsilon_2 > \varepsilon_1)$. This is nothing else but an energy map of the considered dipole in its favorable orientation (note that the dipole favorable orientation depends on the dipole location). Only some of the $(W = \text{const})$-contours that are nearest to the equilibrium dipole position (the star) are depicted. As one can see, there emerges a single minimum point where the dipole is oriented towards the charge Q or in the opposite direction, depending on the Q-sign. Provided the relationship $\varepsilon_1 < \varepsilon_2$ holds, the overall view of this rather simple energy map survives for other p values, but the distance from the energy-minimum point to the interface changes.

The situation when the dipole is located in the same medium with the charge is drastically different (see Fig. 6(b); note that now $\varepsilon_1 > \varepsilon_2$). First, there is no longer a single minimum. Second, the appearance of the minimum has a
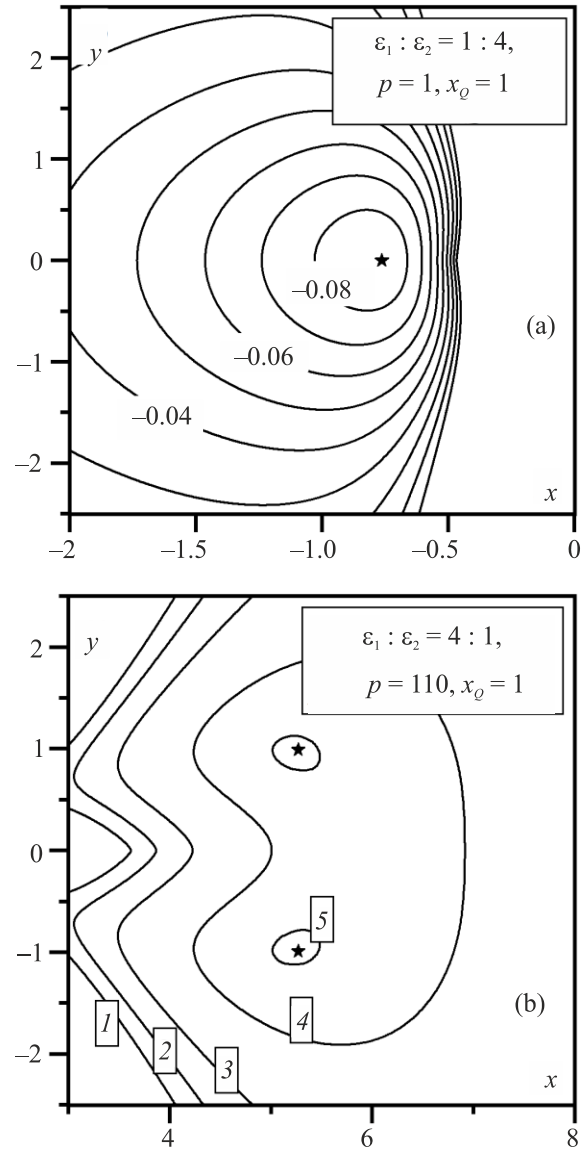

Fig. 6. Contour maps of the dimensionless total energy w of electric dipoles with the indicated parameters (see explanations in the text) in medium 2 (a) and 1 (b). The point charge is located in medium 1. The energy minima are marked by stars. In panel (b), the values of w are as follows: 0 (*1*), $-1 \cdot 10^{-5}$ (*2*), $-2 \cdot 10^{-5}$ (*3*), $-3 \cdot 10^{-5}$ (*4*), and $-3.31 \cdot 10^{-5}$ (*5*).

threshold character. Figure 6(b) illustrates the energy map of the dipole **P** when its reduced magnitude p exceed some critical value (for details, see work [43]). Again, only some of the $(W = \text{const})$-contours that are nearest to the equilibrium dipole positions are displayed. Taking into account that the energy map shown in Fig. 6(b) is the cross-section of a three-dimensional system in the $(z = 0)$-plane, one can see that the two equivalent minima (the stars) represent a ring of stable equilibrium positions of the dipole p around the x axis. Another feature of this configuration is that the dipole-charge interaction tries to orient the dipole along the force lines, whereas the own image forces of the dipole try to orient it in parallel to the interface (because $\varepsilon_1 > \varepsilon_2$).

As a result, the dipole orientation angles with respect to the interface deviate substantially from both the force line at this point and $\pm\pi/2$. In any case, the calculation results testify that we can at least to some extent control the equilibrium distance of the dipole from the interface by changing some problem parameters, which is important for applications, in particular, when dipoles represent excitons.

4. Discussion and conclusions

This article and the related published research on the trampoline ion-flow surface sputtering and structuring once more confirms the fruitful practical consequences of the fundamental curiosity-driven science [83–85], even if it is hidden behind the routine (at the first glance!) scientific activity. In our case, the high-density low-energy ion flow destroys such a large fraction of bonds per time unit at the target surface that a non-equilibrium quasi-liquid state emerges in the near-surface layers of the irradiated target [47, 61]. The phenomenon was found to be inherent to both metals and semiconductors. Since the interaction between the ions targeting the surface and the knocked-out ions (or charged clusters) of the surface material is Coulomb-like, the processes of the local surface erosion can be considered as a Coulomb micro-explosion [86]. The non-equilibrium quasi-liquid state is to a certain extent similar to the equilibrium quasi-liquid in the water ice surface layers discovered by Faraday [87] (see also Refs. 88, 89), which was later claimed to take place at metal surfaces as well [90, 91]. It should be emphasized that the liquid state itself is not a static homogeneous medium even far away from the transition point into the solid phase. On the contrary, it is non-homogeneous in space and time, being permeated by heterophase fluctuations suggested by Frenkel [92, 93] (see also Refs. 94, 95).

The applied trampoline-mode approach led to new results in the specific problem of silicon surface texturing. Indeed, in all known methods of black silicon creation, structures are formed due to the local removal of material from small surface areas. One of the advantageous features of trampoline technology in the formation of black silicon structures is the outflow of material in the form of nanoclusters, which preserves the composition of the target wafer in the film [30, 82]. Since minimal detrimental disturbances occur in the near-surface active layer of silicon, the high effective lifetime of charge carriers is preserved. In addition to the required spectral characteristics of the reflection coefficient, this makes the structured black silicon wafers suitable for application in photovoltaics.

An important advantage of the trampoline technology is the ability to form black silicon structures on surfaces with the (111) orientation, which is impossible to do by applying the method of anisotropic chemical etching in alkali solutions used in the industrial solar cell production technology [56, 58]. Therefore, the trampoline technology for manufacturing black silicon is expected to be effective for multicrystalline-silicon-based photovoltaic applications. Another great benefit of the trampoline formation of black silicon is its environmental friendliness at all stages of the texturing process which creates a hierarchical structure consisting of a nanoscale relief against a background of submicron elements. The only consumable material that is emitted into the surrounding space is the inert gas argon, which is anyway contained in the Earth's atmosphere and is mainly extracted in industry by the fractional distillation of liquid air in cryogenic air separation units [96, 97]. Briefly speaking, argon is returned back into the air from which it was extracted earlier.

The electrostatic interaction between a fixed constant electric charge and a fixed but freely rotating permanent point-like dipole in a simplified two-layer system was calculated. It was shown that the energy minima for the dipole can appear at certain distances from the interface. Dipoles can be considered as models of electron-hole excitons, the quenching of which may determine the total recombination rate of charge carriers in semiconductor layers of solar cells.

Appendix: The birth of hole concept

The treatment of empty electron states in the valence band as holes (positive quasi-particles) has its interesting history. It began when the band theory of periodic solids with non-interacting electrons ("one-electron approximation") was started by Felix Bloch [98] after Arnold Sommerfeld had generalized [99, 100] the classical Paul Drude metal theory [101, 102] by taking into account the Enrico Fermi–Paul Dirac statistics [103, 104] intrinsic to degenerate charge carriers. The interference of electron waves scattered by the periodic crystal potential leads to the appearance of energy gaps between the valence and conductance bands. In this case, the possibility of semiconductors with no intrinsic electric conductivity at zero temperature, $T = 0$, stems from one-dimensional models [105, 106] and the more sophisticated three-dimensional theory of Alan Wilson [107, 108].

At finite T, free negatively charged electrons appear in the conductivity band and create empty states in the va-

lence band. These non-occupied states may be considered as positive particles with certain effective masses. Furthermore, these states can behave as real charged particles; in particular, they can move to cathodes in electric circuits. It was first understood by Rudolf Peierls when theoretically analyzing galvanomagnetic effects in solids and revealing the anomalous positive sign of charge carriers [109]. Those, to some extent fictitious, particles were later named by Ralph Fowler as "occupied holes" [110, 111]. Strictly speaking, both electrons and holes in metals or semiconductors are quasi-particles "dressed" by the environment [112–114].

Nevertheless, the first (earlier!) identification of a vacancy in the medium as a hypothetical particle belongs to Jakov Frenkel [115] (see also Ref. 116). It was applied to remove massive ions in ionic crystals rather than to light electrons in semiconductors. However, this concept was later applied to charge carriers in semiconductors. Now, both the idea and the analogy between those phenomena seem trivial but, nevertheless, it took at least seven years for this approach to become more or less conventional. The indicated case shows once more the utility of analogies in science, in particular, in physics [117–119].

———————

1. J. S. Kilby, *Invention of the integrated circuit*, *IEEE Trans. Electron Devices* **23**, 648 (1976).

2. C. H. Ahn, A. Bhattacharya, M. Di Ventra, J. N. Eckstein, C. D. Frisbie, M. E. Gershenson, A. M. Goldman, I. H. Inoue, J. Mannhart, A. J. Millis, A. F. Morpurgo, D. Natelson, and J. M. Triscone, *Electrostatic modification of novel materials*, *Rev. Mod. Phys*. **78**, 1185 (2006).

3. J. Bardeen and W. H. Brattain, *The transistor, a semiconductor triode*, *Phys. Rev*. **74**, 230 (1947).

4. W. Shockley, *The theory of p–n junctions in semiconductors and p–n junction transistors*, *Bell Syst. Techn. J.* **28**, 435 (1949).

5. W. Shockley, *Electrons and Holes in Semiconductors with Applications to Transistor Electronics*, D. Van Nostrand Company, Inc., Princeton, NJ (1950).

6. W. Shockley, M. Sparks, and G. K. Teal, *p–n junction transistors*, *Phys. Rev*. **83**, 151 (1951).

7. I. M. Ross, *The invention of the transistor*, *Proc. IEEE* **86**, 7 (1998).

8. I. M. Ross, *The foundation of the silicon age*, *Bell Labs Techn. J.* **2**, 3 (2002).

9. D. Esseni, M. Pala, P. Palestri, C. Alper, and T. Rollo, *A review of selected topics in physics based modeling for tunnel field-effect transistors*, *Semicond. Sci. Technol*. **32**, 083005 (2017).

10. A. P. Ramirez and B. Skinner, *Dawn of the topological age*?, *Phys. Today* **73**, 30 (2020).

11. S. Wang, X. Liu, and P. Zhou, *The road for 2D semiconductors in the silicon age*, *Adv. Mater*. **34**, 2106886 (2021).

12. A. Luque, *Will we exceed 50% efficiency in photovoltaics*?, *J. Appl. Phys*. **110**, 031301 (2011).

13. G. D'Avino, L. Muccioli, F. Castet, C. Poelking, D. Andrienko, Z. G. Soos, J. Cornil, and D. Beljonne, *Electrostatic phenomena in organic semiconductors: fundamentals and implications for photovoltaics*, *J. Phys.: Condens. Matter* **28**, 433002 (2016).

14. J. Bisquert, *The Physics of Solar Cells. Perovskites, Organics, and Photovoltaic Fundamentals*, CRC Press, Boca Raton (2018).

15. J. Y-H. Chai, B. T. Wong, and S. Juodkazis, *Black-silicon-assisted photovoltaic cells for better conversion efficiencies: a review on recent research and development efforts*, *Mater. Today Energy* **18**, 100539 (2020).

16. Z. Wang, Y. Hu, S. Zhang, and Y. Sun, *Artificial photosynthesis systems for solar energy conversion and storage: platforms and their realities*, *Chem. Soc. Rev.* **51**, 6704 (2022).

17. A. W. D. Larkum, *Limitations and prospects of natural photosynthesis for bioenergy production*, *Curr. Opinion Biotech.* **21**, 271 (2010).

18. R. van Grondelle and E. Boeker, *Limits on natural photosynthesis*, *J. Phys. Chem. B* **121**, 7229 (2017).

19. D. H. Macdonald, A. Cuevas, M. J. Kerr, C. Samundsett, D. Ruby, S. Winderbaum, and A. Leo, *Texturing industrial multicrystalline silicon solar cells*, *Sol. Energy* **76**, 277 (2004).

20. Z. Huang, N. Geyer, P. Werner, J. de Boor, and U. Gösele, *Metal-assisted chemical etching of silicon: A review*, *Adv. Mater*. **23**, 285 (2010).

21. Z. Zhang, Z. Wang, D. Wang, and Y. Ding, *Periodic antireflection surface structure fabricated on silicon by four-beam laser interference lithography*, *J. Laser Appl.* **26**, 012010 (2014).

22. X. Liu, P. R. Coxon, M. Peters, B. Hoex, J. M. Cole, and D. J. Fray, *Black silicon: fabrication methods, properties and solar energy applications*, *Energy Environ. Sci.* **7**, 3223 (2010).

23. B. Kafle, J. Scön, C. Fleischmann, S. Werner, A. Wolf, L. Clochard, E. Duffy, M. Hofmann, and J. Rentsch, *On the emitter formation in nanotextured silicon solar cells to achieve improved electrical performances, Sol. Energy Mater. Sol. Cells* **152**, 94 (2016).

24. V. A. Milichko, A. S. Shalin, I. S. Mukhin, A. E. Kovrov, A. A. Krasilin, A. V. Vinogradov, P. A. Belov, and K. R. Simovskii, *Solar photovoltaics: current state and trends*, *Phys. Usp.* **59**, 727 (2016).

25. D. Lausch, J. Hirsch, and N. Bernhard, *Plasma texturing of silicon wafers and finished solar cells for mass production*, in: *2018 IEEE 7th World Conference on Photovoltaic Energy Conversion (WCPEC) (A Joint Conference of 45th IEEE PVSC, 28th PVSEC and 34th EU PVSEC), IEEE*, New York (2018), p. 36.

26. L. C. Andreani, A. Bozzola, P. Kowalczewski, M. Liscidini, and L. Redorici, *Silicon solar cells: toward the efficiency limits*, *Adv. Phys. X* **4**, 1548305 (2019).

27. Q. Tan, F. Lu, C. Xue, W. Zhang, L. Lin, and J. Xiong, *Nano-fabrication methods and novel applications of black silicon*, *Sens. Actuators A* **295**, 560 (2019).

28. C. Huo, J. Wang, H. Fu, X. Li, Y. Yang, H. Wang, A. Mateen, G. Farid, and K-Q. Peng, *Metal-assisted chemical etching of silicon in oxidizing HF solutions: origin, mechanism, development, and black silicon solar cell application*, *Adv. Funct. Mater.* **30**, 2005744 (2018).

29. D. K. Ghosh, S. Bose, G. Das, S. Acharyya, A. Nandi, S. Mukhopadhyay, and A. Sengupta, *Fundamentals, present status and future perspective of TOPCon solar cells: A comprehensive review*, *Surf. Interf.* **30**, 101917 (2022).

30. V. N. Gorshkov, M. O. Stretovych, V. F. Semeniuk, M. P. Kruglenko, N. I. Semeniuk, V. I. Styopkin, A. M. Gabovich, and G. K. Boiger, *Hierarchical structuring of black silicon wafers by ion-flow-stimulated roughening transition: fundamentals and applications for photovoltaics*, *Nanomater.* **13**, 2715 (2023).

31. W. Shockley and H. J. Queisser, *Detailed balance limit of efficiency of p–n junction solar cells*, *J. Appl. Phys.* **32**, 510 (1961).

32. T. Tiedje, E. Yablonovitch, G. D. Cody, and B. G. Brooks, *Limiting efficiency of silicon solar cells*, *IEEE Trans. Electron. Devices* **31**, 711 (1984).

33. C. Deibel and V. Dyakonov, *Polymer-fullerene bulk heterojunction solar cells*, *Rep. Prog. Phys.* **73**, 096401 (2010).

34. S. M. Menke and R. J. Holmes, *Exciton diffusion in organic photovoltaic cells*, *Energy Environ. Sci.* **7**, 499 (2014).

35. M. Palummo, M. Bernardi, and J. C. Grossman, *Exciton radiative lifetimes in two-dimensional transition metal dichalcogenides*, *Nano Lett.* **15**, 2794 (2015).

36. A. Classen, C. L. Chochos, L. Lüer, V. G. Gregoriou, J. Wortmann, A. Osvet, K. Forberich, I. McCulloch, T. Heumüller, and C. J. Brabec, *The role of exciton lifetime for charge generation in organic solar cells at negligible energy-level offsets*, *Nat. Energy* **5**, 711 (2020).

37. M. Jain, D. Gill, P. Bhumla, P. Basera, and S. Bhattacharya, *Theoretical insights to excitonic effect in lead bromide perovskites*, *Appl. Phys. Lett.* **118**, 192103 (2021).

38. V. I. Yudson, M. G. Rozman, and P. Reineker, *Bound states of two particles confined to parallel two-dimensional layers and interacting via dipole-dipole or dipole-charge laws*, *Phys. Rev. B* **55**, 5214 (1997).

39. K.-D. Zhu and W.-S. Li, *Bound states of dipole-two charge complex*, *Phys. Lett. A* **252**, 63 (1999).

40. L. Chen, Q. Zhang, Y. Lei, F. Zhu, B. Wu, T. Zhang, G. Niu, Z. Xiong, and Q. Song, *Photocurrent generation through electron-exciton interaction at the organic semiconductor donor/acceptor interface*, *Phys. Chem. Chem. Phys.* **15**, 16891 (2013).

41. W. A. Koopman, M. Natali, G. P. Donati, M. Muccini, and S. Toffanin, *Charge-exciton interaction rate in organic field-effect transistors by means of transient photoluminescence electromodulated spectroscopy*, *ACS Photonics* **4**, 282 (2017).

42. H. Kesavan, S. Sahoo, S. Jena, J. Bhattacharyya, and D. Ray, *Spatial extent of interaction between excitons and polarons in a bilayer organic field-effect transistor*, *ACS Photonics* **8**, 804 (2021).

43. A. M. Gabovich, V. N. Gorshkov, V. F. Semeniuk, and A. I. Voitenko, *Influence of image forces on charge-dipole interaction in two-layered systems*, *J. Chem. Phys.* **160**, 184710 (2024).

44. V. M. Loktev and Yu. G. Pogorelov, *Peculiar physical properties and the colossal magnetoresistance of manganites (Review)*, *Fiz. Nizk. Temp.* **26**, 231 (2000) [*Low Temp. Phys.* **26**, 171 (2000)].

45. V. M. Loktev and V. Turkowski, *Superconducting properties of a two-dimensional doped semiconductor*, *Fiz. Nizk. Temp.* **36**, 1244 (2010) [*Low Temp. Phys.* **36**, 1004 (2010)].

46. Yu. G. Pogorelov and V. M. Loktev, *Biased doped silicene as a way to tune electronic conduction*, *Phys. Rev. B* **93**, 045117 (2016).

47. A. M. Gabovich, V. F. Semeniuk, and N. I. Semeniuk, *New collective trampoline mechanism of accelerated ion-plasma sputtering*, *J. Phys. D* **52**, 185201 (2019).

48. H. Yasuda, *Organo transition metal initiated living polymerizations*, *Prog. Polym. Sci.* **25**, 573 (2000).

49. C. Chiew, M. J. Morris, and M. H. Malakooti, *Functional liquid metal nanoparticles: synthesis and applications*, *Mater. Adv.* **2**, 7799 (2021).

50. X. Xiang and H. Zhu, *One-dimensional gallium nitride micro/nanostructures synthesized by a space-confined growth technique*, *Appl. Phys. A* **87**, 651 (2007).

51. F. F. Chen, *Helicon discharges and sources: a review*, *Plasma Sources Sci. Technol.* **24**, 014001 (2015).

52. A. W. Trivelpiece and R. W. Gould, *Space charge waves in cylindrical plasma columns*, *J. Appl. Phys.* **30**, 1784 (1959).

53. N. A. Krall and A. W. Trivelpiece, *Principles of Plasma Physics*, McGraw-Hill, New York (1973).

54. K. P. Shamrai and V. B. Taranov, *Volume and surface rf power absorption in a helicon plasma source*, *Plasma Sources Sci. Technol.* **5**, 474 (1996).

55. G. G. Borg and R. W. Boswell, *Power coupling to helicon and Trivelpiece–Gould modes in helicon sources*, *Phys. Plasmas* **5**, 564 (1998).

56. R. E. Oosterbroek, J. W. Berenschot, H. V. Jansen, A. J. Nijdam, G. Pandraud, A. van den Berg, and M. C. Elwenspoek, *Etching methodologies in ⟨111⟩-oriented silicon wafers*, *J. Microelectromech. Syst.* **9**, 390 (2000).

57. Ü. Sökmen, A. Stranz, S. Fündling, H.-H. Wehmann, V. Bandalo, A. Bora, M. Tornow, A. Waag, and E. Peiner, *Capabilities of ICP-RIE cryogenic dry etching of silicon: review of exemplary microstructures*, *J. Micromech. Microeng.* **19**, 105005 (2009).

58. *Photovoltaic Manufacturing. Etching, Texturing, and Cleaning*, M. F. Müller (ed.), John Wiley and Sons, Hoboken, NJ (2021).

59. P. Zhang, H. Tian, J. Liu, Y. Zhao, X. Cao, and D. Yu, *Anisotropic etching behavior and topography formation*

mechanism of silicon solar cell surface textured by atmospheric plasma, *J. Appl. Phys.* **135**, 063301 (2024).

60. K. Oura, V. G. Lifshits, A. A. Saranin, A. V. Zotov, and M. Katayama, *Surface Science. An Introduction*, Springer Verlag, Berlin (2003).

61. A. M. Gabovich, V. F. Semeniuk, and N. I. Semeniuk, *Effect of trampoline sputtering on surface morphology and coatings properties*, *J. Phys. D* **54**, 255301 (2021).

62. P. C. Tortorici and M. A. Dayananda, *Growth of silicides and interdiffusion in the* Mo–Si *system*, *Metallurg. Mater Trans. A* **30**, 545 (1999).

63. D. S. Lambert, A. Lennon, and P. A. Burr, *Diffusion mechanisms of* Mo *contamination in* Si, *Phys. Rev. Mater.* **4**, 025403 (2020).

64. A. Rohatgi and P. Rai-Choudhury, *High-efficiency silicon solar cells: Development, current issues and future directions*, *Solar Cells* **17**, 119 (1986).

65. R. N. Hall, *Electron-hole recombination in germanium*, *Phys. Rev.* **87**, 387 (1952).

66. W. Shockley and W. T. Read, Jr., *Statistics of the recombinations of holes and electrons*, *Phys. Rev.* **87**, 835 (1952).

67. W. van Roosbroeck and W. Shockley, *Photon-radiative recombination of electrons and holes in germanium*, *Phys. Rev.* **94**, 1558 (1954).

68. G. Bemski, *Recombination in semiconductors*, *Proc. IRE* **46**, 990 (1958).

69. D. K. Schroder, *Carrier lifetimes in silicon*, *IEEE Trans. Electron. Devices* **44**, 160 (1997).

70. H. J. Queisser, *Detailed balance limit for solar cell efficiency*, *Mater. Sci. Eng. B* **159–160**, 322 (2009).

71. T. Rahman, R. S. Bonilla, A. Nawabjan, P. R. Wilshaw, and S. A. Boden, *Passivation of all-angle black surfaces for silicon solar cells*, *Sol. Energy Mater. Sol. Cells* **160**, 444 (2017).

72. Y. Xu, H. Yao, L. Ma, J. Wang, and J. Hou, *Efficient charge generation at low energy losses in organic solar cells: a key issues review*, *Rep. Prog. Phys.* **83**, 082601 (2020).

73. V. P. Kostylyov, A. V. Sachenko, T. V. Slusar, and V. V. Chernenko, *Reduction of recombination losses in near-surface diffusion emitter layers of photosensitive silicon n^+-p-p^+ structures*, *Ukr. J. Phys.* **68**, 628 (2023).

74. Y. V. Gomeniuk, Y. Y. Gomeniuk, S. V. Kondratenko, T. E. Rudenko, A. V. Vasin, A. V. Rusavsky, O. M. Slobodian, I. P. Tyagulskyy, V. P. Kostylyov, V. M. Vlasiuk, S. I. Tiagulskyi, R. Yatskiv, V. S. Lysenko, and A. N. Nazarov, *Effect of PEDOT:PSS layer deposition on electrical and photoelectrical properties of n^+-ZnO/n-Si heterostructure*, *J. Electron. Mater.* **52**, 3112 (2023).

75. P. Laukkanen, M. Punkkinen, M. Kuzmin, K. Kokko, X. Liu, B. Radfar, V. Vähänissi, H. Savin, A. Tukiainen, T. H. J. Vihrälä, and M. Guina, *Bridging the gap between surface physics and photonics*, *Rep. Prog. Phys.* **87**, 044501 (2024).

76. R. S. Nakhmanson and L. K. Popov, *Measurements of small-signal photo-EMF of* Si *and* Ge *MIS structures using scanning light probe*, *Phys. Status Solidi A* **46**, 59 (1978).

77. *Microanalysis of Solids*, B. G. Yacobi, D. B. Holt, and L. L. Kazmerski (eds.), Springer Verlag, New York (1994).

78. P. van der Heide, *Secondary Ion Mass Spectrometry. An Introduction to Principles and Practices*, John Wiley and Sons, Hoboken, NJ (2014).

79. W. E. Spear, *Doped amorphous semiconductors*, *Adv. Phys.* **26**, 811 (1977).

80. H. J. Möller, T. Kaden, S. Scholz, and S. Würzner, *Improving solar grade silicon by controlling extended defect generation and foreign atom defect interactions*, *Appl. Phys. A* **96**, 207 (2009).

81. I. O. Kruhlov, I. A. Vladymyrskyi, O. Dubikovskyi, S. I. Sidorenko, T. Ebisu, K. Kato, O. Sakata, T. Ishikawa, Y. Iguchi, G. A. Langer, Z. Erdélyi, and S. M. Voloshko, *Oxidation and reduction processes in* Ni/Cu/Cr/Si*(100) thin films under low-energy ion irradiation*, *Mater. Res. Express* **6**, 126431 (2019).

82. A. M. Gabovich, O. Yo. Gudymenko, V. P. Kladko, P. M. Lytvyn, Iu. M. Nasieka, B. M. Romaniuk, V. F. Semeniuk, N. I. Semeniuk, V. V. Strelchuk, V. I. Styopkin, and V. M. Tkach, *Nanosized structure formation by trampoline ion-plasma sputtering*, *Nanosist. Nanomater. Nanotehnol.* **18**, 357 (2020).

83. N. Rosenberg and R. R. Nelson, *American universities and technical advance in industry*, *Res. Policy* **23**, 323 (1994).

84. E. P. Berman, *Creating the Market University. How Academic Science Became an Economic Engine*, Princeton University Press, Princeton, NJ (2012).

85. J. Agar, *2016 Wilkins–Bernal–Medawar lecture. The curious history of curiosity-driven research*, *Notes Rec. Royal Soc.* **71**, 409 (2017).

86. M. O. Vasylyev and B. M. Mordyuk, *The role of Coulomb explosion in the initiation of deformation cracks* (*discussion report*), *Metallofiz. Noveish. Tekhnol.* **46**, 71 (2024).

87. M. Faraday, *Note on regelation*, *Proc. Roy. Soc.* **10**, 440 (1859–1860).

88. J. G. Dash, H. Fu, and J. S. Wettlaufer, *The premelting of ice and its environmental consequences*, *Rep. Prog. Phys.* **58**, 115 (1995).

89. R. Rosenberg, *Why is ice slippery?*, *Phys. Today* **58**, 50 (2005).

90. E. T. Chen, R. N. Barnett, and U. Landman, *Surface melting of* Ni(110), *Phys. Rev. B* **41**, 439 (1990).

91. A. Landa, P. Wynblatt, H. Häkkinen, R. N. Barnett, and U. Landman, *Equilibrium interphase interfaces and premelting of the* Pb(110) *surface*, *Phys. Rev. B* **51**, 10972 (1995).

92. J. Frenkel, *A general theory of heterophase fluctuations and pretransition phenomena*, *J. Chem. Phys.* **7**, 538 (1939).

93. J. Frenkel, *Kinetic Theory of Liquids,* Dover Publications, Mineola, New York (1955).

94. A. R. Ubbelohde, *Melting and crystal structure*, *Quart. Rev. Chem. Soc.* **4**, 356 (1950).

95. V. I. Yukalov, *Phase transitions and heterophase fluctuations*, *Phys. Rep.* **208**, 395 (1991).

96. D. N. Finkelshtein, *Inert Gases,* Nauka, Moscow (1979).

97. X. Jin, A. Malek, and S. Farooq, *Production of argon from an oxygen-argon mixture by pressure swing adsorption, Ind. Eng. Chem. Res.* **45**, 5775 (2006).

98. F. Bloch, *Über die Quantenmechanik der Elektronen in Kristallgittern*, *Z. Phys.* **52**, 555 (1929).

99. A. Sommerfeld, *Zur Elektronentheorie der Metalle auf Grund der Fermischen Statistik. I. Teil: Allgemeines, Strömungs- und Austrittsvorgänge, Z. Phys.* **47**, 1 (1928).

100. A. Sommerfeld, *Zur Elektronentheorie der Metalle auf Grund der Fermischen Statistik. II. Teil: Thermo-elektrische, galvano-magnetische und thermo-magnetische Vorgänge*, *Z. Phys.* **47**, 43 (1928).

101. P. Drude, *Zur Elektronentheorie der Metalle*, *Ann. der Phys.* **306**, 566 (1900).

102. P. Drude, *Zur Elektronentheorie der Metalle; II. Teil. Galvanomagnetische und thermomagnetische Effecte*, *Ann. der Phys.* **308**, 369 (1900).

103. E. Fermi, *Zur Quantelung des idealen einatomigen Gases*, *Z. Phys.* **36**, 902 (1926).

104. P. A. M. Dirac, *On the theory of quantum mechanics*, *Proc. Roy. Soc. A* **112**, 661 (1926).

105. R. Peierls, *Zur Theorie der elektrischen und thermischen Leitfähigkeit von Metallen*, *Ann. der Phys.* **396**, 121 (1930).

106. R. de L. Kronig and W. G. Penney, *Quantum mechanics of electrons in crystal lattices*, *Proc. Roy. Soc. A* **130**, 499 (1931).

107. A. H. Wilson, *The theory of electronic semiconductors,* *Proc. Roy. Soc. A* **133**, 458 (1931).

108. A. H. Wilson, *The theory of electronic semiconductors. II*, *Proc. Roy. Soc. A* **134**, 277 (1931).

109. R. Peierls, *Zur Theorie der galvanomagnetischen Effekte*, *Z. Phys.* **53**, 255 (1929).

110. R. H. Fowler, *An elementary theory of electronic semi-conductors, and some of their possible properties*, *Proc. Roy. Soc. A* **140**, 505 (1933).

111. R. H. Fowler, *Notes on some electronic properties of conductors and insulators*, *Proc. Roy. Soc. A* **141**, 56 (1933).

112. M. Imada, A. Fujimori, and Y. Tokura, *Metal-insulator transitions*, *Rev. Mod. Phys.* **70**, 1040 (1998).

113. C. M. Varma, Z. Nussinov, and W. van Saarloos, *Singular or non-Fermi liquids*, *Phys. Rep.* **361**, 267 (2002).

114. M. Vojta, *Lattice symmetry breaking in cuprate superconductors: stripes, nematics, and superconductivity*, *Adv. Phys.* **58**, 699 (2009).

115. J. Frenkel, *Über die Wärmebewegung in festen und flüssigen Körpern*, *Z. Phys.* **35**, 652 (1926).

116. J. Frenkel, *Conduction in poor electronic conductors, Nature* **132**, 312 (1933).

117. H. F. Olson, *Dynamical Analogies*, D. Van Nostrand Company, Inc., New York (1944).

118. P. Achinstein, *Models, analogies, and theories, Phil. Sci.* **31**, 328 (1964).

119. Y. Gingras, *The creative power of formal analogies in physics: the case of Albert Einstein, Sci. Educ.* **24**, 529 (2015).

Чорний кремній: формування іонного потоку в батутному режимі, властивості поверхні та перспективи застосування

Alexander M. Gabovich, Vitaliy P. Kostylyov, Mykhailo P. Kruglenko, Valerii F. Semeniuk, Nadiia I. Semeniuk, Sergei I. Sidorenko, Victor I. Styopkin, Alexander I. Voitenko, Svitlana M. Voloshko

При опромінюванні поверхні (111) монокристалічних кремнієвих пластин іонами Ar⁺ в батутному режимі (потоки низькоенергетичних іонів великої густини) та за участю атомів металів-ініціаторів відбувається перехід цих пластин у «чорний» оптичний стан кремнію. Цей стан характеризується низькими значеннями світловідбиття (менше ніж 2%) з боку опромінюваної пластини в спектральному інтервалі від 400 до 1000 нм. Дослідження за допомогою скануючої електронної мікроскопії показали, що це є результатом появи ієрархічної субмікрон/нанорозмірної структури на обробленій поверхні пластин. Цей перехід є можливим лише за участю атомів металу-ініціатора, які одночасно розпилюються з допоміжної мішені в робочій камері. Водночас застосування металів-ініціаторів впливає на ефективний час життя неосновних носіїв заряду в чорному кремнії, що є вирішальним для ефективності застосування чорного кремнію в сонячних елементах. Серед досліджуваних металів-ініціаторів (Al, Cr, Fe, Ni, Mo, Cu) лише застосування міді дозволило зберегти або навіть збільшити значення цього параметра. Теоретично розглянуто електростатичну взаємодію між вільними електричними зарядами та диполями (в цьому випадку останні моделюють екситони) поблизу межі розділу у двошаровій системі. Показано, як параметри системи впливають на переважне розташування екситонів та їхню орієнтацію, що можна застосувати, наприклад, для керування ефективністю сонячного елемента. Формування чорного кремнію в батутному режимі є екологічно чистим на всіх етапах виробництва.

Ключові слова: іонно-плазмовий потік, напівпровідники, фотовольтаїка, чорний кремній, екситони, диполі, дзеркальні сили.